

Thermal axion production

Alberto Salvio,^a Alessandro Strumia^{b,c} and Wei Xue^d

^a *Departamento de Física Teórica, Universidad Autónoma de Madrid and Instituto de Física Teórica IFT-UAM/CSIC, Cantoblanco, 28049 Madrid, Spain*

^b *Dipartimento di Fisica dell'Università di Pisa and INFN, Italia*

^c *National Institute of Chemical Physics and Biophysics, Tallinn, Estonia*

^d *INFN, Sezione di Trieste, SISSA, via Bonomea 265, 34136 Trieste, Italy*

Abstract

We reconsider thermal production of axions in the early universe, including axion couplings to all Standard Model (SM) particles. Concerning the axion coupling to gluons, we find that thermal effects enhance the axion production rate by a factor of few with respect to previous computations performed in the limit of small strong gauge coupling. Furthermore, we find that the top Yukawa coupling induces a much larger axion production rate, unless the axion couples to SM particles only via anomalies.

Contents

1	Introduction	2
2	Outline of the computation	3
2.1	Effective axion Lagrangian	3
2.2	Thermal production rate	4
3	Subtracted scattering rates	6
4	Thermal vector decays	9
4.1	Thermal corrections to vector propagators	10
4.2	Axion production via vector thermal decays	11
5	Result	12
5.1	Cosmological axion yield	13
6	Conclusions	15

1 Introduction

The strong CP problem can be solved by a Peccei-Quinn (PQ) symmetry [1], that manifests at low energy as a light axion a . The axion is a good dark matter (DM) candidate, if cold axions are produced non-thermally via the initial misalignment mechanism [2]. The cosmological DM abundance is reproduced for an order one initial misalignment angle provided that $f_a \approx 10^{11}$ GeV, which is compatible with the experimental bound $f_a \gtrsim 5 \times 10^9$ GeV [3, 4]. The ADMX experiment can probe such scenario in the next years [5].

Furthermore, thermal scatterings in the early universe unavoidably produce a population of hot axions. The goal of this paper is performing an improved computation of hot axion thermal production. The thermal axion production rate [6] was previously computed in [7] making use of the Hard Thermal Loop (HTL) [8, 9] approximation ($g_3 \ll 1$), and considering only the axion coupling to gluons. The resulting space-time density of thermal axion production was:

$$\gamma_a^{\text{HTL}} = \frac{\zeta(3)g_3^4 T^6}{64\pi^7 f_a^2} F_3^{\text{HTL}}, \quad F_3^{\text{HTL}} = g_3^2 \ln \frac{1.5^2}{g_3^2}. \quad (1.1)$$

However, this HTL production rate unphysically decreases for $g_3 \gtrsim 1.3$ becoming negative for $g_3 \gtrsim 1.5$. Fig. 1 shows that the physical value, $g_3 \approx 0.85$ at $T \sim 10^{10}$ GeV, lies in the region where the HTL rate function $F_3^{\text{HTL}}(g_3)$ (lower dashed line) is unreliable. Fig. 1 also illustrates our final result: as described in the following sections, F_3^{HTL} will be replaced by F_3 , plotted in the upper line, which agrees with the HTL result in the limit $g_3 \ll 1$, and is about twice larger for the physical value of g_3 .

Furthermore, we go beyond the anomalous axion coupling to gluons (a loop level effect), computing the axion production rate due to all axion couplings. We find that the axion coupling to top quarks (a tree level effect) gives an axion production rate which is about 3 orders of magnitude larger, unless the axion couples to SM particles only via anomalies

In section 2 we outline our computation, performed in section 3 (subtracted scattering rates) and in section 4 (higher order enhanced effects). In section 5 we present our final result and discuss its cosmological implications. Conclusions are presented in section 6. An off-topic but important subtlety is discussed in a footnote.¹

¹We show that scattering involving many particles can be neglected. This is trivially true in quantum field theory: for example the cross section for $2 \rightarrow 3$ scatterings is $g^2/(4\pi)^2$ times smaller than the cross section of the dominant $2 \rightarrow 2$ scatterings. However, this is not generically true in thermal field theory, where the expansion parameter is g (rather than $g^2/(4\pi)^2$) and where collinear kinematical configurations can enhance higher order scatterings by powers of $1/g$, such that a resummation of $2 \rightarrow n$ scattering becomes needed. This subtlety was noticed in the context of computations of photon emission from a quark-gluon plasma [10]: for example, the $2 \rightarrow 3$ process constructed adding to a $qg \rightarrow qg$ scattering a $q \rightarrow q\gamma$ vertex, where q and γ are almost collinear (the directions of their moment differ by a small angle θ) allows a kinematical configuration where the propagator of the virtual gluon that mediates the scattering is enhanced by $1/\theta^2$, while the gauge vertex $q \rightarrow q\gamma$ is only suppressed by θ . This results into a $1/\theta$ enhancement of the scattering amplitude, cut-off by the thermal mass $m \sim gT$, and thereby to a $1/g^2$ enhancement of the $2 \rightarrow 3$ scattering rate.

We verified that no such collinear enhancement is present for axion production, because the axion vertices (such as the axion/gluon/gluon vertex $aG_{\mu\nu}\tilde{G}_{\mu\nu}$) are suppressed as θ^2 in the collinear limit. We also verified that the similar vertices relevant for graviton, gravitino [14], axino [15] production similarly lead to no collinear enhancement, being θ^2 suppressed. Thereby there is no need of adding higher order scatterings and previous computations remain valid.

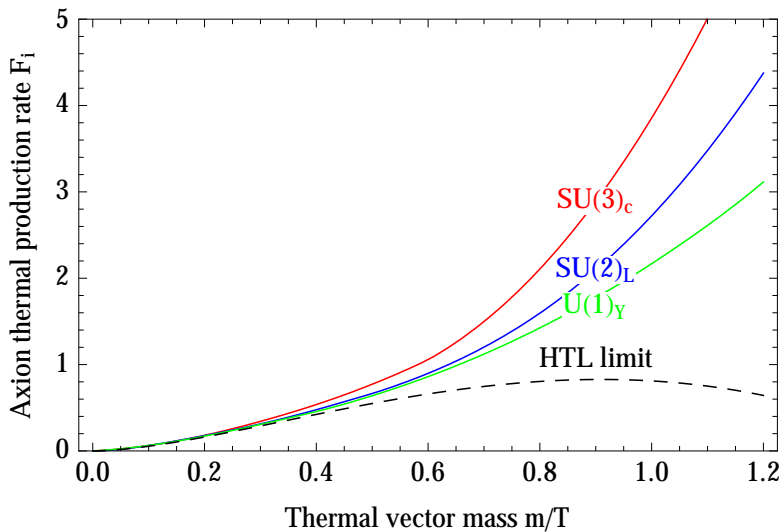


Figure 1: Our result for the axion production rate as function of the thermal mass of vectors. The functions $F_{1,2,3}(m/T)$ are defined in eq. (5.1) and the thermal masses of the vectors within the SM are $m/T = g_3$ for gluons, $m/T = \sqrt{11/12}g_2$ for the W, Z and $m/T = \sqrt{11/12}g_Y$ for hypercharge. For comparison, the lower dashed curve is the result of [7] (eq. (1.1)) computed within the HTL approximation, valid in the limit $g_3 \ll 1$.

2 Outline of the computation

2.1 Effective axion Lagrangian

The effective action that describes axion couplings to SM particles at first order in the axion field a is written in the basis where the SM Lagrangian \mathcal{L}_{SM} does not contain the axion as [1]

$$\begin{aligned} \mathcal{L} = & \mathcal{L}_{\text{SM}} + \frac{(\partial_\mu a)^2}{2} - \frac{a}{f_a} \left[c_3 \frac{\alpha_3}{8\pi} G_{\mu\nu}^a \tilde{G}_{\mu\nu}^a + c_2 \frac{\alpha_2}{8\pi} W_{\mu\nu}^a \tilde{W}_{\mu\nu}^a + c_1 \frac{\alpha_Y}{8\pi} B_{\mu\nu} \tilde{B}_{\mu\nu} \right] + \\ & + \frac{\partial_\mu a}{f_a} \left[c_H H^\dagger i(D_\mu H) - c_H i(D_\mu H)^\dagger H \right] + \frac{\partial_\mu a}{f_a} \sum_\psi c_\psi (\bar{\psi} \gamma_\mu \psi). \end{aligned} \quad (2.1)$$

Here $\tilde{G}_{\mu\nu} = \frac{1}{2}\varepsilon_{\mu\nu\alpha\beta}G_{\alpha\beta}$ are the field strength duals; $\varepsilon_{0123} = 1$; H is the Higgs doublet; the Weyl spinors $\psi = \{Q, U, D, L, E\}$ are the SM fermions; f_a is the effective axion decay constant in the convention where $c_3 = 1$; c_1 and c_2 are the axion couplings to electro-weak vectors; c_H is the axion coupling to the Higgs; c_ψ are the axion derivative couplings to the SM fermions. All c coefficients are real and dimensionless. In the full axion theory c_H and c_ψ are the PQ charges of the SM fields (they vanish in KSVZ axion models [3]), while $c_{1,2,3}$ also receive contributions from extra heavy fermions (not present in DFSZ axion models [4]).²

²As usual, the effective action above is reliable only at energies much below the masses of the extra non-SM fields present in the axion model one considers. For example, if the KSVZ extra fermions with non-vanishing PQ charges were light enough to be present in the thermal bath, they would give an extra contribution to the

While in previous computations only the axion/gluon coupling was considered, we want to consider all axion couplings.

For this purpose, it is convenient to perform a phase redefinition of the SM matter fields

$$\psi \rightarrow e^{ic_\psi a/f_a} \psi, \quad H \rightarrow e^{ic_H a/f_a} H \quad (2.2)$$

such that, at the first order in a , the c_ψ and c_H couplings are removed, at the price of shifting the axion coupling to vectors as follows

$$\begin{aligned} c_3 &\rightarrow c'_3 \equiv c_3 + \sum (c_U + c_D - 2c_Q), \\ c_2 &\rightarrow c'_2 \equiv c_2 - \sum (3c_Q + c_L), \\ c_1 &\rightarrow c'_1 \equiv c_1 + \sum (2c_E - c_L + \frac{8}{3}c_U + \frac{2}{3}c_D - \frac{1}{3}c_Q), \end{aligned} \quad (2.3)$$

where the sum runs over the 3 fermion generations. We used the fact that all SM matter field lie in fundamental representations with generators T^a normalized as $\text{Tr}(T^a T^b) = \delta^{ab}/2$. The transformation (2.2) also introduces an axion phase in the SM Yukawa couplings. For our purposes, all SM Yukawa couplings are negligibly small except the top Yukawa, for which the transformation induces the following axion phase:

$$y_t \rightarrow y_t \exp \left[ic'_t \frac{a}{f_a} \right], \quad c'_t \equiv c_H + c_{Q_3} - c_{U_3}. \quad (2.4)$$

So, at first order in a , the transformation generates the following Lagrangian interaction:

$$ic'_t y_t \frac{a}{f_a} Q_3 H U_3 + \text{h.c.} \quad (2.5)$$

The thermal axion production rate will be computed in terms of c'_3 (strong interactions), c'_2 (weak interactions), c'_1 (hypercharge) and c'_t (top Yukawa coupling).

2.2 Thermal production rate

According to the general formalism of thermal field theory [9], the thermal production rate of a weakly interacting scalar a is equivalently computed from the imaginary part of its propagator Π_a as

$$\gamma_a = \frac{dN_a}{dV dt} = -2 \int d\vec{P} f_B(E) \text{Im} \Pi_a = \int d\vec{P} \Pi_a^<(P), \quad d\vec{P} \equiv \frac{d^3 p}{2E(2\pi)^3}. \quad (2.6)$$

Here $\Pi_a^<$ is the non time-ordered axion propagator and $P = (E, \vec{p})$. Thermal field theory cutting rules allow to see that, at leading order in the SM couplings, eq. (2.6) is equivalent to the usual summing of all rates for the various tree-level processes that lead to axion production.

We illustrate the general discussion with the concrete example of the axion coupled to a simplified SM consisting only of gluons. In such a case the thermal axion production rate γ at leading order in g_3 can be obtained by computing the $gg \rightarrow ga$ scattering rate and thermally averaging it.

axion production rate at tree level, that would dominate with respect to one-loop contribution that we consider, encoded in the anomaly coefficients $c_{1,2,3}$. The computation of such extra contribution would be analogous to the top Yukawa contribution discussed below.

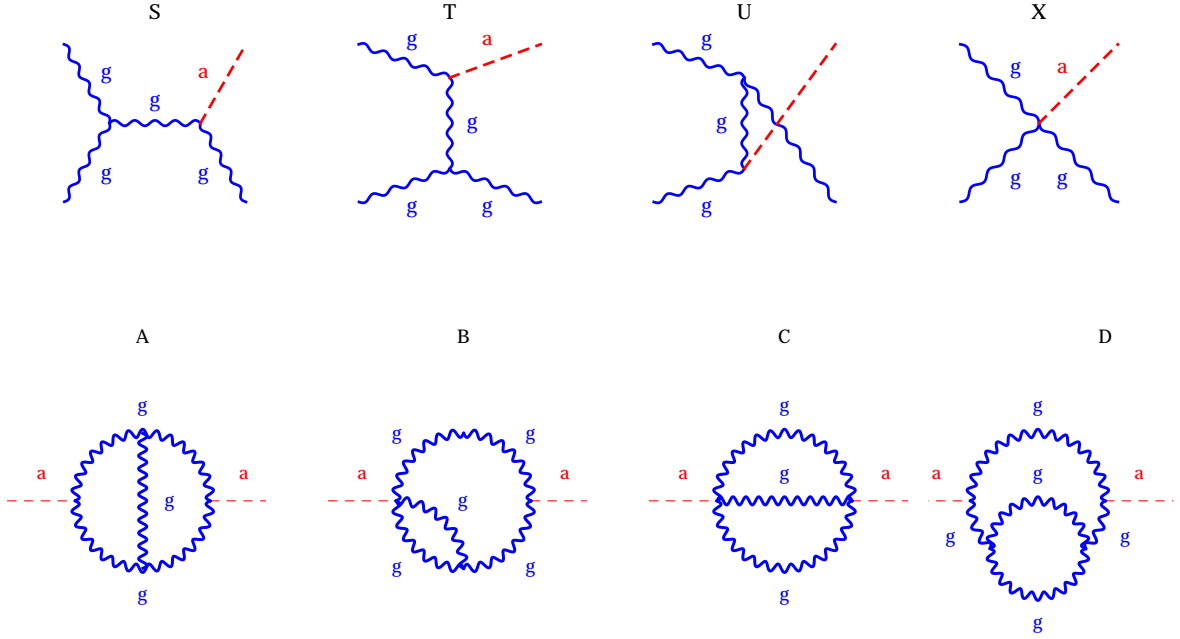


Figure 2: *The leading-order $gg \rightarrow ga$ scattering rate in the thermal plasma is equivalently obtained by: a) summing the Feynman diagrams in the upper row, squaring the total amplitude, performing the thermal average; b) summing the imaginary parts of the two loop thermal diagrams in the lower row. In both cases the result is infra-red divergent, such that proper inclusion of higher order effects is needed. For simplicity, we here plotted the diagrams relative to a simplified world without quarks.*

- The Feynman diagrams for $gg \rightarrow ga$ scatterings are plotted in the upper row of figure 2 and are named S (s -channel gluon exchange), T (t -channel), U (u -channel) and X (quartic vertex). When computing the rate in terms of scatterings, the rate is proportional to the modulus squared of the total amplitude, $|S + T + U + X|^2$.
- The equivalent thermal diagrams at leading order in g_3 arise at two-loop level and are plotted in the lower row of figure 2, where they are named A , B , C , D . The rate is proportional to their sum, that contains the various tree-level scatterings in the following way:

$$\begin{aligned}
 A &= 2\text{Re}[S^*T + S^*U + T^*U] & B &= 2\text{Re}[X^*(S + T + U)], \\
 C &= |X|^2 & D &= |S|^2 + |T|^2 + |U|^2.
 \end{aligned}
 \tag{2.7}$$

We explicitly see that the thermal axion production rate $\gamma = \gamma_A + \gamma_B + \gamma_C + \gamma_D$ is equivalent to the scattering computation $|S + T + U + X|^2$.

However, both computations give an infra-red divergent result, because of the massless gluon in the T and U diagrams, or equivalently in the thermal diagram D . We employ the thermal field theory formalism because it is more appropriate for dealing with such issues.

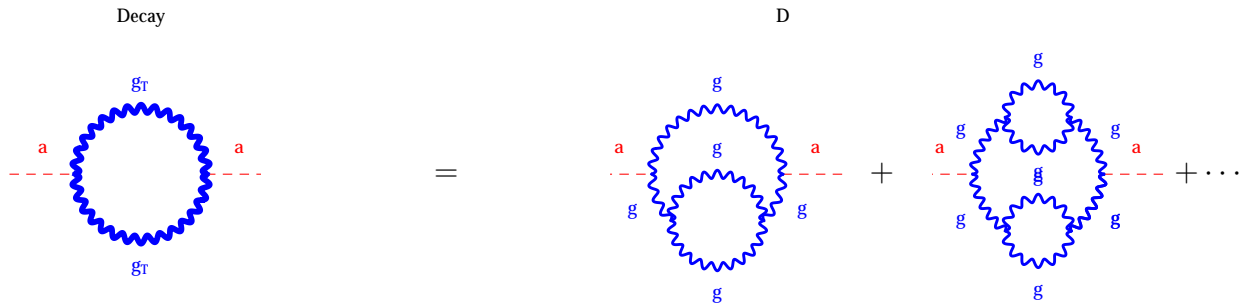


Figure 3: *The thermal diagram ‘Decay’, where the gluon propagator includes one-loop thermal corrections, is equivalent to the thermal diagram D (thick lines denote the propagator of the thermal gluon g_T) plus the resummation of higher order diagrams with corrections to the gluon propagator.*

The infra-red divergence is regulated by the thermal gluon mass. We re-sum the thermal effects that modify the gluon dispersion relation by substituting the two-loop thermal diagram D with the one-loop ‘Decay’ diagram of fig. 3, where the tree-level gluon propagator is replaced by the full thermal gluon propagator at leading order in the strong coupling. In a diagrammatic expansion, the ‘Decay’ diagram corresponds to diagram D , plus all higher order diagrams with any number of corrections to the gluon propagator, as illustrated in the right-handed side of figure 3. We give the name ‘decay’ to such resummed diagram because physically it describes the decay process $g_T \rightarrow g_T a$ of the thermal gluon g_T , opened by the non-relativistic thermal corrections to the gluon propagator. The rationale for re-summing this class of higher-order effects is that they are enhanced by the $2 \rightarrow 1$ phase space factor, which is $\sim (4\pi)^2$ bigger than the phase space relative to $2 \rightarrow 2$ scatterings.

In conclusion, the resummed total axion production rate is computed as

$$\gamma = \gamma_A + \gamma_B + \gamma_C + \gamma_{\text{Decay}} \equiv \gamma_{\text{sub}} + \gamma_{\text{Decay}}. \quad (2.8)$$

The computation of γ_{sub} (subtracted scattering rates) is presented in section 3, and the computation of γ_{Decay} is presented in section 4. Unlike in the HTL approximation, our technique does not need the introduction of an arbitrary splitting scale k_* that satisfies the problematic conditions $g_3 T \ll k_* \ll T$ in order to control infra-red divergences. The total rate will be positive for any g_3 .

While we omitted quarks and other axion couplings to simplify the above discussion, of course we take them into account in the full computation.

3 Subtracted scattering rates

Table 1 lists the full scattering rates and the subtracted scattering contributions to the various axion production processes due to the axion/gluon/gluon interaction. It is important to notice

that, unlike the total rate, *the subtracted rates are infra-red convergent* as expected: the infra-red divergent factors $1/t$ and $1/u$ present in the full rate disappear from the subtracted rate. Actually, by performing computations in the Feynman gauge, we find that $\gamma_{\text{sub}} = 0$. The same holds for the other SM vectors.

In order to double-check our result, we computed the subtracted scattering rates also as thermal diagrams that contribute to the non time-ordered axion propagator $\Pi_a^<$, see eq. (2.6). This computation is presented in the next part of this section. At the end of this section we also evaluate the top Yukawa contribution, which emerges from the axion interaction term in (2.5).

Diagram A

We first consider the contribution of the thermal diagram A in fig. 2. Making use of the Kobes-Semenoff rules (see e.g. [11]) we obtain the following contribution of the diagram A to $\Pi^<$:

$$\Pi_A^< = F \int \frac{d^4 K}{(2\pi)^4} \int \frac{d^4 Q}{(2\pi)^4} \Delta^<(P-K) \Delta^<(K-Q) \Delta^<(Q) \text{Re} [\Delta(K) \Delta(P-Q)^*] \alpha(P, K, Q), \quad (3.9)$$

where $F \equiv 2c_i^2 g_i^6 / [3(4\pi)^4 f_a^2]$, P is the axion momentum and Δ and $\Delta^<$ are respectively the tree level scalar propagator and non time-ordered propagator at finite temperature:

$$\Delta(K) = \frac{i}{K^2 + i\epsilon} + 2\pi n_B(K_0) \delta(K^2), \quad \Delta^<(K) = (\theta(-K_0) + n_B(K_0)) 2\pi \delta(K^2), \quad (3.10)$$

where $n_B(x) \equiv (\exp(|x|/T) - 1)^{-1}$. These emerge from the scalar part of the gluon propagators, while the contraction of Lorentz and color indices leads to the function α defined by

$$\alpha(P, K, Q) \equiv C_N [4(Q \cdot P)^2 (K \cdot P - 4K^2) - 2K \cdot PQ \cdot P (K^2 + Q^2 - 14K \cdot Q - 2K \cdot P) - 16Q^2 (K \cdot P)^2], \quad (3.11)$$

where we have introduced $C_N \equiv N(N^2 - 1)$ with $N = 3, 2, 1$ for $\text{SU}(3)_c$, $\text{SU}(2)_L$ and $\text{U}(1)_Y$ respectively. Looking at the thermal diagram we find that the kinematical configurations with non vanishing phase space in the integrand of eq. (3.9) are

1. $P_0 - K_0 < 0, \quad Q_0 > 0, \quad K_0 - Q_0 > 0;$
2. $Q_0 < 0, \quad P_0 - K_0 > 0, \quad K_0 - Q_0 > 0;$
3. $K_0 - Q_0 < 0 \quad Q_0 > 0, \quad P_0 - K_0 > 0.$

As anticipated in eq. (2.7), these contributions correspond to the interferences between the s -channel, t -channel and u -channel scattering diagrams. Although these contributions are separately non-trivial, we find that their sum is identically zero. So $\Pi_A^< = 0$.

process	$ \mathcal{A} ^2/(g_3^6/128\pi^2 f_a^2)$	$ \mathcal{A} _{\text{sub}}^2/(g_3^6/128\pi^2 f_a^2)$
$gg \rightarrow ga$	$-4 f^{abc} ^2(s^2 + st + t^2)/st(s+t)$	0
$q\bar{q} \rightarrow ga$	$ T_{ji}^a ^2(s + 2t + 2t^2/s)$	0
$qg \rightarrow qa$	$ T_{ji}^a ^2(-t - 2s - 2t^2/s)$	0

Table 1: Axion production rate from the axion/gluon/gluon interaction. The total rate is gauge independent; the subtracted rate is gauge dependent and computed in the Feynman gauge.

Diagram B

We now turn to the thermal diagram B in fig. 2. We find:

$$\Pi_B^< = 4F \int \frac{d^4 K}{(2\pi)^4} \int \frac{d^4 Q}{(2\pi)^4} \Delta^<(K) \Delta^<(Q) \Delta^<(P - K - Q) \text{Im} [\Delta(P - K)] \beta(P, Q, K). \quad (3.12)$$

The function β , which results from the contraction of Lorentz and color indices, is

$$\beta(P, Q, K) \equiv 3C_N [K \cdot P (K \cdot P + 2K \cdot Q + 2Q \cdot P) - 2K^2 Q \cdot P]. \quad (3.13)$$

The phase space of the integrand in (3.12) can be divided in three regions, which correspond to the interferences between the x -channel and the s , t and u -channels respectively:

1. $K_0 < 0$, $Q_0 > 0$, $P_0 - K_0 - Q_0 > 0$;
2. $Q_0 < 0$, $K_0 > 0$, $P_0 - K_0 - Q_0 > 0$;
3. $P_0 - K_0 - Q_0 < 0$, $Q_0 > 0$, $K_0 > 0$.

The sum of the three contributions in the phase space gives zero like for Diagram A: $\Pi_B^< = 0$.

Diagram C

Finally, we evaluate the thermal diagram C in fig. 2, the contribution of the x -channel alone. It contributes to $\Pi^<$ an amount

$$\Pi_C^< = 18FC_N \int \frac{d^4 K}{(2\pi)^4} \int \frac{d^4 Q}{(2\pi)^4} \Delta^<(K) \Delta^<(Q) \Delta^<(P - K - Q) P \cdot Q. \quad (3.14)$$

Like for thermal diagrams A and B we can divide the phase space in three parts, which this times correspond to the possibility to choose one out of three gluons and put it in the final state. The sum of these three contributions vanishes like for diagram A and B: $\Pi_C^< = 0$.

The top Yukawa contribution

The axion interaction in eq. (2.5) produces the following contribution to $\Pi_a^<$ at the first non-trivial order in the perturbative expansion

$$\Pi_t^< = -24 \left(\frac{c_t y_t}{f_a} \right)^2 \int \frac{d^4 K}{(2\pi)^4} \int \frac{d^4 Q}{(2\pi)^4} Q \cdot P \Delta_F^<(K) \Delta_F^<(P - K - Q) \Delta^<(Q), \quad (3.15)$$

where Δ_F^{\leq} is the tree level non time-ordered propagator at finite temperature for a fermion:

$$\Delta_F^{\leq}(K) \equiv [\theta(-K_0) - n_F(K_0)]2\pi\delta(K^2) \quad (3.16)$$

and $n_F(x) \equiv (\exp(|x|/T) + 1)^{-1}$. Like in the previous computation, the integral receives contributions from three distinct integration regions, which correspond to the effects that can be equivalently computed as $Q_3H^* \rightarrow a\bar{U}_3$, $U_3H^* \rightarrow a\bar{Q}_3$ and $Q_3U_3 \rightarrow aH$ scatterings (as well as their CP-conjugated processes):

1. $K_0 < 0$, $P_0 - K_0 - Q_0 > 0$, $Q_0 > 0$;
2. $K_0 > 0$, $P_0 - K_0 - Q_0 < 0$, $Q_0 > 0$;
3. $K_0 > 0$, $P_0 - K_0 - Q_0 > 0$, $Q_0 < 0$.

The first possibility, for example, leads to the following contribution to the production rate

$$\gamma_{t1} = \frac{6c_t'^2 y_t^2}{(2\pi)^6 f_a^2} \int dp dk dz_k dq dz_q p^2 q (1 - z_q) \frac{(1 - n_F(k))n_F(p + k - q)n_B(q)}{D_1(k, q, z_k, z_q)^{1/2}}, \quad (3.17)$$

where the integral is performed on the intersection between the domains

$$0 \leq p < \infty, \quad 0 \leq k < \infty, \quad -1 \leq z_k \leq 1, \quad 0 \leq q < \infty, \quad -1 \leq z_q \leq 1 \quad (3.18)$$

and

$$D_1(k, q, z_k, z_q) \equiv (1 - z_k)(1 - z_q) - \left[-1 - z_k z_q + \frac{p}{q}(1 + z_k) - \frac{p}{k}(1 - z_q) \right]^2 \geq 0. \quad (3.19)$$

These conditions emerge because k and q are the lengths of the three dimensional parts (\vec{k} and \vec{q}) of the on shell momenta K and Q , once the delta functions in (3.16) are used, and z_k and z_q are the cosines of the angles between \vec{k} and \vec{p} and \vec{q} and \vec{p} respectively.

The other two contributions lead to similar expressions. The total result due to the interaction in (2.5) is

$$\gamma_a^{\text{top}} = 0.94 \frac{3y_t^2 c_t'^2 T^6}{2\pi^5 f_a^2}, \quad (3.20)$$

where the numerical factor is the Bose-Einstein and Fermi-Dirac correction with respect to the analytic result computed in Boltzmann approximation, $n_{B,F}(E) \approx e^{-E/T}$.

4 Thermal vector decays

We start summarizing some well known results from quantum field theory at finite temperature that are relevant for our computations.

4.1 Thermal corrections to vector propagators

We list the full one-loop expressions for thermal corrections to a vector [12, 13, 9] with four-momentum $K = (\omega, \vec{k})$ ($K^2 = \omega^2 - k^2$) with respect to the rest frame of the thermal plasma. We denote by U_μ the four-velocity U_μ of the plasma. We use the Feynman gauge where all effects are condensed in two form factors even in the non-abelian case [12]. Polarizations are conveniently decomposed in *Transverse* (i.e. orthogonal to K and to \vec{k}), *Longitudinal* (i.e. orthogonal to K and parallel to \vec{k}) and parallel to K . The corresponding projectors $(\Pi^T + \Pi^L + \Pi^K)_{\mu\nu} = -\eta_{\mu\nu}$ are

$$\Pi_{\mu\nu}^T = -\tilde{\eta}_{\mu\nu} + \frac{\tilde{K}_\mu \tilde{K}_\nu}{-k^2} = \begin{pmatrix} 0 & 0 \\ 0 & \delta_{ij} - k_i k_j / k^2 \end{pmatrix}, \quad (4.1a)$$

$$\Pi_{\mu\nu}^L = -\eta_{\mu\nu} + \frac{K_\mu K_\nu}{K^2} - \Pi_{\mu\nu}^T, \quad (4.1b)$$

$$\Pi_{\mu\nu}^K = -\frac{K_\mu K_\nu}{K^2}, \quad (4.1c)$$

where $\tilde{\eta}_{\mu\nu} = \eta_{\mu\nu} - U_\mu U_\nu$, $\tilde{K}_\mu = K_\mu - (K \cdot U)U_\mu$. The vector propagator is [12, 13]

$${}^*D_{\mu\nu} = i \left[\frac{\Pi_{\mu\nu}^T}{K^2 - \pi_0 - \pi_T} + \frac{\Pi_{\mu\nu}^L}{K^2 - \pi_0 - \pi_L} + \frac{\Pi_{\mu\nu}^K}{K^2} \right] \quad (4.2)$$

where the corrections are contained in the scalar functions $\pi_0(k, \omega)$ (quantum corrections at $T = 0$) and $\pi_T(k, \omega)$ and $\pi_L(k, \omega)$ (thermal corrections), explicitly given in [14] for a general theory. The corresponding non-time ordered propagator is

$${}^*D_{\mu\nu}^<(K) = f_B(k_0) \left[\Pi_{\mu\nu}^T \rho_T(K) + \Pi_{\mu\nu}^L \frac{|\mathbf{k}|^2}{K^2} \rho_L(K) + \xi \frac{k_\mu k_\nu}{K^4} \right]. \quad (4.3)$$

Here, ρ_T, ρ_L are the spectral densities for the transverse vectors and longitudinal vectors respectively

$$\rho_T = -2 \operatorname{Im} \frac{1}{K^2 - \pi_0 - \pi_T}, \quad \rho_L = -2 \operatorname{Im} \frac{K^2}{k^2} \frac{1}{K^2 - \pi_0 - \pi_L}. \quad (4.4)$$

Furthermore, $k_0 > 0$ describes a vector in the final state, and $k_0 < 0$ describes a vector in the initial state: this convention allows to compactly describe all possible processes. Indeed the factors

$$f_B(k_0) \equiv \frac{1}{e^{k_0/T} - 1} = \begin{cases} n_B(k_0) & \text{if } k_0 > 0 \\ -(1 + n_B(k_0)) & \text{if } k_0 < 0 \end{cases} \quad (4.5)$$

gives the usual statistical factors: $-n$ (number of particles in the initial state) or $1 \pm n$ (stimulated emission or Pauli-blocking in the final state), where $n_B(E) \equiv 1/(e^{|E|/T} - 1)$ is the Bose-Einstein distribution.

Fig. 4 shows the spectral densities in the HTL limit ($g \ll 1$, left panels) and in a realistic situation ($g \sim 1$, right panels). In the realistic case, the poles get smeared acquiring a finite width. A more significant difference arises below the light cone ($\omega < k$), where both the HTL and the one-loop spectral densities do not vanish. This describes ‘Landau damping’ i.e. the fact that particles exchange energy with the thermal plasma. However, the HTL approximation cannot be applied at $k \sim T$ (a region relevant for us, since $g \sim 1$), and indeed it misses that at $k \gg T$ spectral densities get suppressed by an exponential Boltzmann factor.

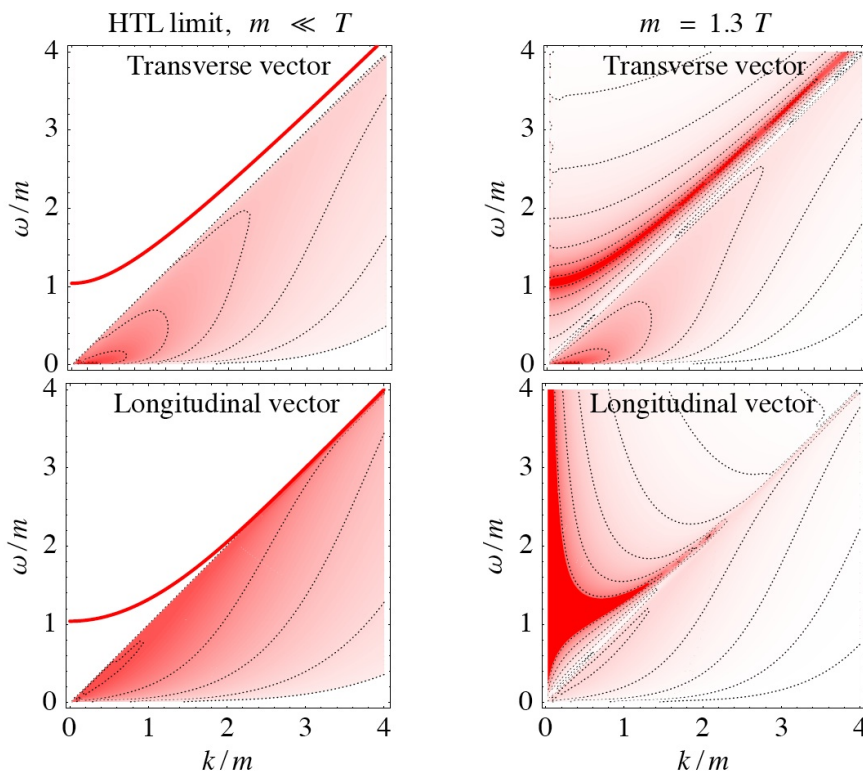


Figure 4: One loop thermal densities $\rho_T(\omega, k)$ (upper row) and $\rho_L(\omega, k)$ (lower row) for a vector in the Hard Thermal Loop limit $g \ll 1$ (left) and for $g \sim 1$ (right). In the HTL limit there is a pole above the light cone and a continuum below the light cone. In the full case the pole above the light cone acquires a finite width and becomes a continuum, and the continuum below the light cone gets Boltzman suppressed at $k \gg m$.

4.2 Axion production via vector thermal decays

In section 3 we have computed the subtracted axion production rate; we here compute the resummed ‘Decay’ diagram of fig. 3, which reduces at leading order to diagram D in fig. 2. As already stated, the rationale for re-summing only this class of higher-order effects is the phase space enhancement of the $2 \rightarrow 1$ processes (relative to the $2 \rightarrow 2$ scatterings). Therefore, the residual gauge dependence in our result is expected to be of relative order g^2/π^2 . The computation applies to all SM vectors $V = \{g, W, Y\}$ with gauge couplings $\alpha_i = \{\alpha_3, \alpha_2, \alpha_Y\}$ and dimension of the gauge group $d_i = \{8, 3, 1\}$.

The resummed contribution to the axion propagator $\Pi_a^<$ is

$$\Pi_{\text{res}}^< = \frac{c_i^2 d_i \alpha_i^2}{f_a^2 8\pi^2} \int \frac{d^4 K}{(2\pi)^4} \epsilon^{\mu\nu\alpha\beta} \epsilon^{\mu'\nu'\alpha'\beta'} K_\alpha Q_\beta K_{\alpha'} Q_{\beta'} {}^*D_{\mu\mu'}^<(K) {}^*D_{\nu\nu'}^<(Q), \quad (4.6)$$

The vector quadri-momenta are K_μ and $Q_\mu = P_\mu - K_\mu$, where P_μ is the axion quadri-momentum. Inserting the parametrization

$$P = (p_0, p, 0, 0), \quad K = (k_0, k \cos \theta_k, k \sin \theta_k, 0), \quad Q = (q_0, q \cos \theta_q, q \sin \theta_q, 0), \quad (4.7)$$

Gauge group	N	N_F	N_S	Thermal mass ²
Color SU(3) _c	3	6	0	$g_3^2 T^2$
Weak SU(2) _L	2	6	1/2	$11g_2^2 T^2/12$
Hypercharge U(1) _Y	0	10	1/2	$11g_Y^2 T^2/12$

Table 2: Numerical coefficients for vector thermal mass $m_i^2 = \frac{1}{6}g_i^2 T^2(N + N_S + N_F/2)$ in the SM in terms of the SU(N) factor, of the number of fermions N_F and of scalars N_S .

we obtain

$$\begin{aligned} \Pi_{\text{res}}^{\leq} &= \frac{c_i'^2 d_i \alpha_i^2}{f_a^2 8\pi^2} \int \frac{d^4 K}{(2\pi)^4} f_B(k_0) f_B(q_0) \times \\ &\left\{ (\rho_L(K) \rho_T(Q) + \rho_T(K) \rho_L(Q)) k^2 q^2 \sin^2(\theta_k - \theta_q) + \right. \\ &\left. \rho_T(K) \rho_T(Q) [(k_0^2 q^2 + k^2 q_0^2) (1 + \cos^2(\theta_k - \theta_q)) - 4k_0 q_0 k q \cos(\theta_k - \theta_q)] \right\}, \quad (4.8) \end{aligned}$$

where we used the decomposition of the resummed propagator given in (4.3). In order to compute the integral, it is convenient to multiply by $1 = \int d^4 Q \delta(K + Q - P)$. After performing the angular integrations over θ_k and θ_q , and using the equations,

$$\cos \theta_q = \frac{-k^2 + q^2 + p^2}{2pq}, \quad \cos \theta_k = \frac{k^2 - q^2 + p^2}{2kp}, \quad \cos(\theta_k - \theta_q) = \frac{-k^2 - q^2 + p^2}{2kq} \quad (4.9)$$

we obtain

$$\begin{aligned} \Pi_{\text{res}}^{\leq} &= \frac{c_i'^2 d_i \alpha_i^2}{f_a^2 8(2\pi)^5} \frac{1}{p} \int_{-\infty}^{\infty} dk_0 \int_0^{\infty} dk \int_{|k-p|}^{k+p} dq k q f_B(k_0) f_B(p_0 - k_0) \\ &\left\{ (\rho_L(K) \rho_T(Q) + \rho_T(K) \rho_L(Q)) [(k+q)^2 - p^2] [p^2 - (k-q)^2] + \right. \\ &\left. \rho_T(K) \rho_T(Q) \left[\left(\frac{k_0^2}{k^2} + \frac{q_0^2}{q^2} \right) ((k^2 - p^2 + q^2)^2 + 4k^2 q^2) + 8k_0 q_0 (k^2 + q^2 - p^2) \right] \right\}. \quad (4.10) \end{aligned}$$

Note that the integration range is restricted to $|p-k| \leq q \leq p+k$. Finally, for each factor of the SM gauge group we computed this integral numerically using the spectral densities described in the previous section. We followed the method provided in [14].

5 Result

The total axion production rate due to all axion couplings c_3', c_2', c_1', c_t' and taking into account all large SM couplings, g_3, g_2, g_Y, y_t is

$$\gamma_a = \frac{T^6 \zeta(3)}{(2\pi)^5 f_a^2} \left[37c_t'^2 y_t^2 + 8c_3'^2 \alpha_3^2 F_3\left(\frac{m_3}{T}\right) + 3c_2'^2 \alpha_2^2 F_2\left(\frac{m_2}{T}\right) + c_1'^2 \alpha_Y^2 F_1\left(\frac{m_1}{T}\right) \right], \quad (5.1)$$

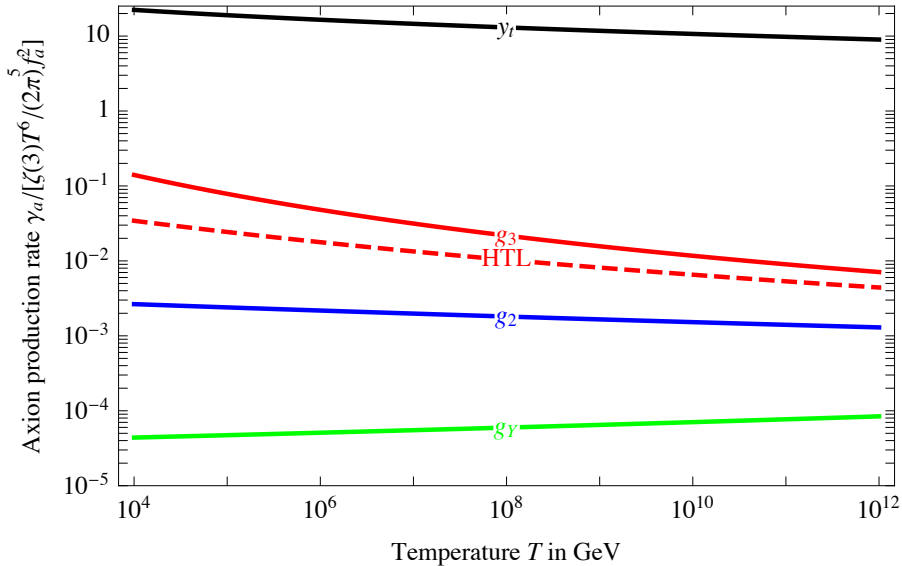


Figure 5: *The four contributions to the thermal axion production rate γ_a induced by the SM couplings y_t (upper black curve), g_3 (red curve), g_2 (blue), g_Y (green) for unity values of the axion couplings $c'_t = c'_3 = c'_2 = c'_1 = 1$ in eq. (5.1). The red dashed line is the previous result for the strong coupling contribution computed in Hard Thermal Loop approximation.*

where the thermal masses of SM gauge bosons of $SU(3)_c$, $SU(2)_L$ and $U(1)_Y$ are (see table 2):

$$\frac{m_3}{T} = g_3, \quad \frac{m_2}{T} = \sqrt{\frac{11}{12}}g_2, \quad \frac{m_1}{T} = \sqrt{\frac{11}{12}}g_Y. \quad (5.2)$$

Fig. 1 shows our results for the functions $F_{1,2,3}$ that parameterize the axion production rate due to gauge interactions, while our result for the top Yukawa part is given analytically. Fig. 5 shows the four contributions to the axion production rate as function of the temperature. As long as $c'_t \sim c'_3$ the top Yukawa axion production rate gives the dominant contribution because it arises at tree level, while the anomalous axion couplings arise at loop level.

Previous works ignored the top Yukawa effect and computed only the function F_3 within the HTL approximation i.e. in the limit of small strong gauge coupling, $g_3 \ll 1$. We see that in this limit our improved computation reproduces to the HTL limit. However, when g_3 is set to its physical value, $g_3 \approx 1$, the results differ: the HTL approximation breaks down and the HTL rate function F_3^{HTL} becomes unphysically negative for a large enough g_3 , while our result grows with increasing g_3 .

5.1 Cosmological axion yield

In the usual scenario of reheating after inflation, the inflaton ϕ with energy density ρ_ϕ decays with width Γ_ϕ into SM particles (excluding the axion). The reheating temperature T_{RH} is defined as the temperature at which Γ_ϕ equals H_R , the expansion rate due to the radiation

density only:

$$T_{\text{RH}} = \left[\frac{45}{4\pi^3 g_*} \Gamma_\phi^2 M_{\text{Pl}}^2 \right]^{1/4}. \quad (5.3)$$

Here we neglect possible non-equilibrium effects at $T \gg T_{\text{RH}}$ [17]. T_{RH} effectively is the maximal temperature of the universe. Indeed, while higher temperatures exist, particles produced at $T > T_{\text{RH}}$ are diluted by the entropy released by inflaton decays, as described by the $Z - 1 = -\Gamma_\phi \rho_\phi / 4H\rho_R$ term in the Boltzmann equations

$$\begin{cases} HZz \frac{d\rho_\phi}{dz} = -3H\rho_\phi - \Gamma_\phi \rho_\phi, \\ sHZz \frac{dY_a}{dz} = 3sH(Z-1)Y_a + \gamma_a \left(1 - \frac{Y_a}{Y_a^{\text{eq}}}\right). \end{cases} \quad (5.4)$$

Here $H = \sqrt{8\pi\rho/3}/M_{\text{Pl}}$ is the Hubble parameter, $z = T_{\text{RH}}/T$, $s = 2T^3 g_{\text{SM}} \pi^2 / 45$ is the entropy density of SM particles ($g_{\text{SM}} = 427/4$), n_a is the axion number density, $Y_a = n_a/s$, and $Y_a^{\text{eq}} = n_a^{\text{eq}}/s \approx 0.00258$ with $n_a^{\text{eq}} = \zeta(3)T^3/\pi^2$ is the thermal equilibrium value of Y_a . The solution to the Boltzmann equations for the axion abundance at $T \ll T_{\text{RH}}$ is

$$\frac{Y_a}{Y_a^{\text{eq}}} = (1 + r^{-3/2})^{-2/3} \simeq \begin{cases} r & \text{for } r \ll 1 \\ 1 & \text{for } r \gg 1 \end{cases} \quad (5.5)$$

where

$$r = \frac{2.4}{Y_a^{\text{eq}}} \frac{\gamma_a}{Hs} \Big|_{T=T_{\text{RH}}} = 1.7 \frac{T_{\text{RH}}}{10^7 \text{ GeV}} \left(\frac{10^{11} \text{ GeV}}{f_a} \right)^2 \frac{\gamma_a}{T^6 \zeta(3)/(2\pi)^5 f_a^2} \Big|_{T=T_{\text{RH}}}. \quad (5.6)$$

The latter factor in eq. (5.6) is the order-one term among square brackets in eq. (5.1). The approximated analytical expression of eq. (5.5) valid for intermediate values of r is obtained by fitting the numerical solution.

Even for the lowest possible value of $f_a \gtrsim 5 \times 10^9 \text{ GeV}$ and taking into account the new top effect in γ_a , eq. (5.6) implies that axions decoupled at $T \gtrsim M_Z$, when the number of relativistic SM degrees of freedom g_{SM} still included all SM particles. Thereby, when SM particles later become non-relativistic, they annihilated heating photons and neutrinos, but not axions. This means that today, and at the epoch of CMB decoupling, thermal axions constitute a small fraction of the total relativistic energy fraction, conveniently parameterised by the usual “effective number of neutrinos” as³

$$\Delta N_\nu^{\text{eff}} = 0.0264 \frac{Y_a}{Y_a^{\text{eq}}}. \quad (5.7)$$

The phenomenological manifestations in cosmology of a thermal axion component of the universe are analogous to having an extra freely-streaming neutrino component. Such effects can be parameterised by the axion contribution to effective number of neutrinos $\Delta N_\nu^{\text{eff}}$ and by the axion mass $m_a \approx 0.6 \text{ meV} (10^{10} \text{ GeV}/f_a)$.

³Today photons have temperature T_γ and neutrinos have temperature $T_\nu = T_0(4/11)^{1/3}$, for a total of $g_{*s} = 43/11$ effective entropy degrees of freedom. Axions went out of thermal equilibrium at $T \gg M_Z$ would have a present temperature $T_a = T_\gamma (g_{*s}/g_{\text{SM}})^{1/3} = 0.903 \text{ K}$, which corresponds to $\Delta N_\nu^{\text{eff}} = 4(T_a/T_\nu)^4/7 \approx 0.0264$. We recall that the SM alone predicts $N_\nu^{\text{eff}} \approx 3.046$ where the small deviation from 3 is due to imperfect neutrino decoupling when electrons become non-relativistic [16].

Full cosmological bounds in the plane $(\Delta N_\nu^{\text{eff}}, m)$ were computed in fig. 6a of [18] and, more recently, in fig. 28 of [19]. In practice, present global fits of cosmological data find $\Delta N_\nu^{\text{eff}} = 0.48 \pm 0.48$ [19]: the uncertainty is more than one order of magnitude above the maximal thermal axion effect. Future experiments which are being discussed, such as CMBpol, can reduce the uncertainty on N_ν^{eff} to ± 0.044 [20].

6 Conclusions

In conclusion, we improved over previous computations of the thermal axion density in two ways:

1. By including higher-order effect enhanced by the thermal decay kinematics gluon \rightarrow gluon + axion. Unlike the leading order result, which becomes negative for $g_3 > 1.5$, our result behaves physically for all relevant values of the strong gauge coupling.
2. By considering all axion couplings to SM particles; not only to gluons. The strong interaction contribution receives new contributions from the axion couplings to quarks, as encoded in the difference between c_3 and c'_3 , eq. (2.3). Electroweak effects are small. More importantly, as long as the axion couples to the top quark, there is a new effect related to the top Yukawa coupling, which dominates by 3 order of magnitude over the effect related to the strong gauge coupling (see fig. 5).

Our result for the thermal axion production rate is given in eq. (5.1) in terms of the axion couplings c'_3 (strong interactions), c'_2 (weak interactions), c'_1 (hypercharge) and c'_t (top Yukawa coupling) defined in eq. (2.3) and (2.5). The thermal functions F_3, F_2, F_1 are numerically plotted in fig. 1.

Furthermore, we have shown that there are no collinear enhancements (in analogous computations such effects are present and require resummation of extra classes of thermal diagrams).

The thermal axion abundance is then computed adopting the usual simplified model of reheating (rather than the instantaneous reheating approximation adopted in previous works) and allowing for the possibility of a thermalised axion. We provide in eq. (5.5) a simple numerical approximation for the final axion abundance.

Acknowledgements We thank Simon Caron-Huot, Gian Giudice, Julien Lesgourgues, Alessandro Melchiorri, for useful discussions and in particular Slava Rychkov for having clarified the physics of collinear enhancements. We thank Daniel Green and Benjamin Wallisch for having pointed out a numerical error in the electroweak gauge contribution in fig. 5, which has been corrected. This work was supported in part by the European Programme PITN-GA-2009-23792 (UNILHC). The work of Alberto Salvio has been supported by the Spanish Ministry of Economy and Competitiveness Consolider-CPAN (CSD2007-00042), the grant SEV-2012-0249 of the ‘‘Centro de Excelencia Severo Ochoa’’ Programme and the grant HEPHACOS-S2009/ESP1473 from the C.A. de Madrid. This work was supported by the ESF grant MTT8 and by SF0690030s09 project.

References

- [1] R. D. Peccei and H. R. Quinn, Phys. Rev. D 16 (1977) 1791. R. D. Peccei and H. R. Quinn, Phys. Rev. Lett. 38 (1977) 1440. S. Weinberg, Phys. Rev. Lett. 40 (1978) 223. F. Wilczek, Phys. Rev. Lett. 40 (1978) 279. H. Georgi, D.B. Kaplan, L.

- Randall, Phys. Lett. 169B (1986) 73. D. B. Kaplan and A. V. Manohar, Phys. Rev. Lett. 56 (1986) 2004.
- [2] J. Preskill, M. Wise, F. Wilczek, Phys. Lett. B120 (1983) 127. L. Abbott and P. Sikivie, Phys. Lett. B120 (1983) 133. M. Dine and W. Fischler, Phys. Lett. B120 (1983) 137.
- [3] J. E. Kim, Phys. Rev. Lett. 43 (1979) 103; M. A. Shifman, V. I. Vainstein, V. I. Zakharov, Nucl. Phys. B166 (1980) 4933.
- [4] M. Dine, W. Fischler and M. Srednicki, Phys. Lett. B104 (1981) 199; A. P. Zhitnitskii, Sov. J. Nucl. Phys. 31 (1980) 260.
- [5] [ADMX website](#).
- [6] E. Masso, F. Rota, G. Zsembinski, Phys. Rev. D66, 023004 (2002). For previous calculations at much lower temperatures see Z.G. Berezhiani, A.S. Sakharov and M.Yu. Khlopov, Yadernaya Fizika 55 (1992) 1918 [english translation: Sov. J. Nucl. Phys. 55 (1992) 1063].
- [7] P. Graf and F. D. Steffen, Phys. Rev. D 83 (2011) 075011 [arXiv:1008.4528].
- [8] E. Braaten, R.D. Pisarski, Phys. Rev. D45 (1992) R1827.
- [9] M. Le Bellac, *Thermal Field Theory*, Cambridge University Press (2000), ISBN 0521654777.
- [10] E. Braaten, T.C. Yuan, Phys. Rev. Lett. 66 (1991) 2183.
- [11] A. Salvio, P. Lodone and A. Strumia, JHEP 1108 (2011) 116 [[1106.2814](#)].
- [12] Vectors at finite temperature. D. J. Gross, R. D. Pisarski and L. G. Yaffe, Rev. Mod. Phys. 53, 43 (1981). H. Weldon, Phys. Rev. D26 (1982) 1394. H. T. Elze, K. Kajantie and T. Toimela, Z. Phys. C 37, 601 (1988). R. Kobes, G. Kunstatter and K. W. Mak, Z. Phys. C 45, 129 (1989). H. Weldon, Annals Phys. 271 (1999) 141 [[hep-ph/9701279](#)].
- [13] A. Peshier, K. Schertler, M. Thoma, Annals Phys. 266 (1998) 162 [[hep-ph/9708434](#)].
- [14] V. S. Rychkov and A. Strumia, Phys. Rev. D 75 (2007) 075011 [[hep-ph/0701104](#)].
- [15] A. Strumia, JHEP 1006 (2010) 036 [[1003.5847](#)].
- [16] For a review and references see A. D. Dolgov, Phys. Rept. 370 (2002) 333 [hep-ph/0202122]. J. Lesgourgues et al., *Neutrino Cosmology*, Cambridge University Press (2013).
- [17] D. J. H. Chung, E. W. Kolb and A. Riotto, Phys. Rev. D **60** (1999) 063504 [hep-ph/9809453]. A. Mazumdar and B. Zaldivar, arXiv:1310.5143 [hep-ph].
- [18] M. Cirelli and A. Strumia, JCAP 0612 (2006) 013 [[astro-ph/0607086](#)].
- [19] Planck collaboration, arXiv:1303.5076.
- [20] S. Galli, M. Martinelli, A. Melchiorri, L. Pagano, B. D. Sherwin and D. N. Spergel, Phys. Rev. D 82 (2010) 123504 [arXiv:1005.3808]. C. Brust, D. E. Kaplan and M. T. Walters, arXiv:1303.5379.